Probing hidden conduction mechanisms in diced silicon solar cells by low frequency noise analysis

Chloé Wulles, Quentin Rafhay, Thibaut Desrues, Anne Kaminski, Christoforos Theodorou

Probing Hidden Conduction Mechanisms in Diced Silicon Solar Cells by Low Frequency Noise Analysis

Chloé Wulles[1], Quentin Rafhay[1], Thibaut Desrues[2], Anne Kaminski[1], Christoforos Theodorou[1]

[1]Univ. Grenoble Alpes, Univ. Savoie Mont Blanc, CNRS, Grenoble INP, IMEP-LAHC, 38000 Grenoble, France
[2]Univ. Grenoble Alpes, CEA, LITEN, DTS, SCPV, F-73370 Le Bourget-du-Lac

***Abstract* - Electrical low frequency noise (LFN) measurements are utilized in this work to identify parasitic low voltage transport mechanisms in diced aluminum back surface field (Al-BSF) photovoltaic (PV) cells. A detailed method for LFN analysis is proposed, taking into account the co-existence of various transport mechanisms usually occurring in parallel in PV components. A precise examination of the *1/f* noise level dependency with both current and voltage, combined with static I-V characterization at various temperatures, enabled the identification of two different flicker noise sources appearing at different current regions: one attributed to local linear shunts and a second one to a fluctuation in a nonlinear parasitic conductivity localized at the samples cut edges. The latter shows a noise signature similar to a transport via tunneling or Poole-Frenkel effect, meanwhile excluding a SRH recombination current. This hypothesis was further verified by measurements of thermal activation energies which were found to be typical of tunnel and Poole-Frenkel conduction mechanisms.**

1 Introduction

The current growth of the photovoltaic market [1], answering current needs for renewable energy sources, encourages the development of tools and methods to characterize precisely the components used in such systems. Photovoltaic (PV) cells performances are known to be limited in particular by defects introduced during their fabrication, which are responsible for recombination of photo-generated carriers, leading to decreased efficiency [2]. Structural defects can also enable parasitic low voltage conduction mechanisms reducing the fill factor of photovoltaic devices [3] and greatly diminishing their performance at low light intensity [4]. These undesired contributions to the current are usually attributed to recombination processes in the depletion region, sometimes with inaccurate ideality factors [5],[6],[7].

The analysis of low frequency noise (LFN) is a non-destructive method widely used to detect and characterize defects in semiconductor devices such as CMOS transistors [8]. Their operation makes them very suitable for noise measurement since the channel conduction is governed by only one type of charge carrier and can be modulated thanks to the gate voltage control. LFN characterization has also been explored in diode structures, but there is a lack of consensus with regards to noise modeling in these components since their operation is usually more complex [9]. Indeed, both electron and hole conductions are involved through various mechanisms in series. PV cell devices, in particular, are even more cumbersome to study since there are also parasitic parallel conduction mechanisms, mainly due to their large size and to the presence of defects induced by cost-saving fabrication processes or dicing/cutting methods [10].

The complexity of these devices therefore forces the use of multiple and benchmarked characterizations, to assess with confidence the nature of the parasitic effects. In this framework, LFN appears as an additional technique in PV studies, under-employed however since the generalization of LFN techniques to multiple mechanisms, although compulsory, has not been developed yet.

This paper presents a methodical approach for the analysis of the LFN measured in Al-BSF PV cells, in presence of multiple types of transport mechanisms. A first section will introduce theoretical bases regarding noise in semiconductor devices, and present a condensed state of the art of LFN measurements in PV cells, as well as the approach used to model *1/f* noise results in this work. In the second section, the samples structure and the measurement set up used will be detailed. Experimental results will be exposed and interpreted in the third section.

2 Theoretical approach for 1/f noise analysis in solar cells

2.1 Noise basics and state of the art

Electronic noise designates any random variations around a mean value measured in a current or in a voltage signal. Although this phenomenon is generally unwanted because it is regarded as a perturbation, it can provide unique information about intrinsic fluctuation mechanisms of electronic components. The power spectral density (PSD), giving access to the distribution of a signal power over a frequency bandwidth, is systematically used to analyze noise results. It can be expressed according to the Wiener-Khinchin theorem for a wide-sense stationary process *U* as [11]

$$S_U(f) = \int_{-\infty}^{+\infty} r_{UU}(t) e^{-2i\pi f t} dt \tag{2.1}$$

where r_{UU} is the autocorrelation function of *U*.

Different types of noise can be identified according to their PSD spectrum. The most basic one, designated as *white noise*, stems from physical phenomena whose variations are uncorrelated in time and its PSD spectrum is therefore flat with frequency. Physical processes with an exponential relaxation characterized by a time constant τ produce a *Lorentzian spectrum*, flat at low frequencies and varying as $1/f^2$ for frequencies significantly larger than $1/2\pi\tau$. In most common cases, many processes with different time constants τ occur and the sum of their contribution is measured. In the case that the time constants values obey an exponential distribution, this sum results in a third type of noise called *Flicker noise* or *1/f noise*. This type of noise is very often measured in semiconductor devices, and its current PSD follows:

$$S_I \sim 1/f^{\gamma} \tag{2.2}$$

where γ is a frequency exponent whose value is varying around 1 depending on the uniformity of the time constants distribution for the processes at stake. According to the literature, the *1/f* noise in semiconductors may originate either from a fluctuation of the mobility ($\Delta\mu$) or from a fluctuation of the number of free charge carriers (ΔN). Mobility fluctuations are generally attributed to phonon scattering in the bulk material and modelled by the empirical Hooge's formula [12]. Processes inducing fluctuations in the number of charge carriers, such as electron trapping/de-trapping or Generation-Recombination [13][14] processes can occur either in the bulk or at the interface with an oxide or other material. Since interfaces are known to be preferential zones for crystallographic defects enhancing the occurrence of these processes, the measured LFN is traditionally interpreted with surface-based models, such as the McWhorter one [15].

While LFN has been explored and modelled in diodes and p-n junctions since the 1950s [9], [16], [17], its study in PV cells is more recent. Noise is presented in some works as an indicator of PV cells degradation and as a tool for reliability estimation. The detection of degradation signs in LFN measurements is for example investigated through ageing studies in crystalline silicon-based solar cells in [18]–[20] and in GaAs devices in [21]. The method has been explored in many different PV structures such as silicon heterojunction cells [22], or emerging photovoltaic technologies such as perovskite-based ones [23]–[29], organic ones [30]–[35], or carbon nanotube-based ones[36]. Very recently, the LFN characterization coupled with the atomic force microscopy (AFM) technique has produced remarkable results in [23], further solidifying this method as a very promising non-destructive characterization tool for PV cells.

In the vast majority of the works evoked here however, characterization through LFN is limited to the analysis of PSD spectra, whereas the information hidden in the noise level dependency with current and voltage is rarely fully exploited. This rare use could partially be explained by the lack of published works on the modeling of noise in the case of multiple parallel transport mechanisms inducing several sources of fluctuations. The following subsection will present a first generalization of the noise dependency with current and voltage in such cases.

2.2 Assessing the possible LFN behavior in solar cells

If a time-domain current signal *I*, depending on a parameter *V*, has the following form of dependence:

$$I(V,t) = f(V)X(t) \tag{2.1}$$

where X is a random variable whose fluctuations are supposed to be independent of V and f a time-independent function of V, the PSD of I can be expressed according to Eq. (1.1) as:

$$S_I(f,V) = \int_{-\infty}^{+\infty}\left(\int_{-\infty}^{+\infty} f(V)X(\tau)f(V)X(t-\tau)d\tau\right)e^{-i2\pi ft}dt = f(V)^2 S_X(f) \quad (2.2)$$

In this simplified case, the noise measured will be proportional to I^2 and $f(V)^2$. Thus, in the case of an ohmic conduction mechanism with I_R defined as:

$$I_R(V,t) = G(t)V\ , \quad (2.3)$$

if the time fluctuations of the conductance are inducing *1/f* noise, the power spectral density S_{I_R} in the concerned frequency range is expected to verify both:

$$\begin{cases} S_{I_R}(f) = V^2 S_G(f) \\ S_{I_R}(f) = I^2 R^2 S_G(f) \end{cases} \quad (2.4)$$

Due to their large size and the use of cost-saving processes for their fabrication, PV cells usually feature several conduction mechanisms occurring in parallel. The widely used double diode model [3], given here in dark measurement conditions, describes three parallel conduction mechanisms:

$$I = \frac{(V-IR_S)}{R_{sh}} + I_{S_2}\left(exp\left(\frac{q(V-IR_S)}{n_2 k_b T}\right)\right) + I_{S_1}\left(exp\left(\frac{q(V-IR_S)}{n_1 k_b T}\right)\right) \quad (2.5)$$

where R_S is the series resistance, R_{sh} a parallel resistance modelling shunts due to fabrication defects [37], and I_{S1} and I_{s2} are the dark currents of an ideal diode with an ideality factor n_1 equal to 1 and a second diode modelling recombination processes via SRH mechanism in the space charge zone (SCZ) with an ideality factor n_2 equal to 2, respectively. As indicated in several research works [5]-[6], it is common for n_2 to be found superior to 2 in cut or damaged solar cells and that the low-voltage current, generally resulting from localized effects, cannot always be approximated by this model.

In order to analyze the LFN in solar cells, it is hence essential to take into account these several parallel contributions to the current. If a current signal I is composed for example of two conduction mechanisms and can be written as a function of the voltage V as:

$$I(V,t) = X(t)f(V) + Y(t)g(V) \quad (2.6)$$

where X and Y are two uncorrelated random variables whose fluctuations are independent of V and g and f are two time-independent functions of V, the PSD of this signal can be expressed as:

$$S_I(f,V) = f(V)^2 S_X(f) + g(V)^2 S_Y(f) \quad (2.7)$$

This approach, assuming that the fluctuation sources do not depend on the voltage applied, provides a first approximation tool to analyze noise measurements. This formulation highlights the fact that the measured noise level may not necessarily result from the conduction mechanism dominating the static current, provided that the fluctuation produced in the underlying mechanism is large enough. In a case like that, the dependency of S_I with both I and V can help identify hidden conduction mechanisms, not visible in the DC behavior.

3 Experimental details

3.1 Devices under test

The measured samples are Al-BSF solar cells fabricated at CEA-INES as detailed in [38], laser cut into smaller devices with various rectangular geometries, whose dimensions are presented in table 1. The study was carried out on fifteen samples (three of each size), whose static and noise measurements results are presented in Figure 1.

Table 1 : Geometries of diced solar cells on which noise measurements presented in section III were carried out.

Sample shape	Area (mm^2)	Perimeter (mm)	Area/perimeter (mm)
A	25	20	1.25

B	100	40	2.5
C	25	25	1.00
D	62.5	55	1.14
E	625	100	6.25

Reducing the size of the devices was required to adjust to the set-up current limitations evoked in the following section. Samples dimensions have thus been chosen carefully to study their impact on noise behavior. Similar noise behaviors have also been obtained with other Al-BSF samples not presented in this paper, on which cuts were obtained with diamond saw.

3.2 Measurement setup

The noise measurements have been carried out thanks to the noise acquisition system NOISYS7, developed by SYNERGIE CONCEPT Co., Meylan, France, whose architecture is described in [39]. This equipment is able to perform current noise measurement for currents between 100 pA and 10 mA, on a maximum bandwidth between 1Hz and 100 kHz. This range, very well suited for small components, can be quite limiting in the case of PV cells standard test structures as they induce a parasitic oscillation in the measurement bandwidth as explained in [40], which hence motivated the laser cutting of the device.

4 Experimental results and analysis

This section presents the experimental results and explains the methodology approach applied to these in order to analyze noise sources in these solar cells. As it can be seen in Fig. 1-a, presenting current-voltage curves in log scale for the fifteen samples studied, some parasitic low voltages currents are measured in all cases. Some typical linear shunt currents can be extracted at very low voltage, with a device-to-device variability observed due to the random and local aspect of the defects inducing such parasitic conduction mechanisms. The current normalization with the samples perimeter leads to a gathering of the curves between about 200 mV and 500 mV, therefore enabling the identification of a second conduction mechanism through the edges. The values extracted at *100 Hz* of the *Flicker noise* measured in all samples are presented for each as a function of the applied voltage in Fig 1-b. Different tendencies with voltage, depending both on the samples and the voltage range, can be observed. The noise level is proportional to the square of the voltage for all samples under 100 mV and this dependence is gradually increased at higher bias for certain samples. A precise analysis and modeling of these different behaviors will be performed in what follows, based on three particular samples exhibiting the most pronounced behaviors.

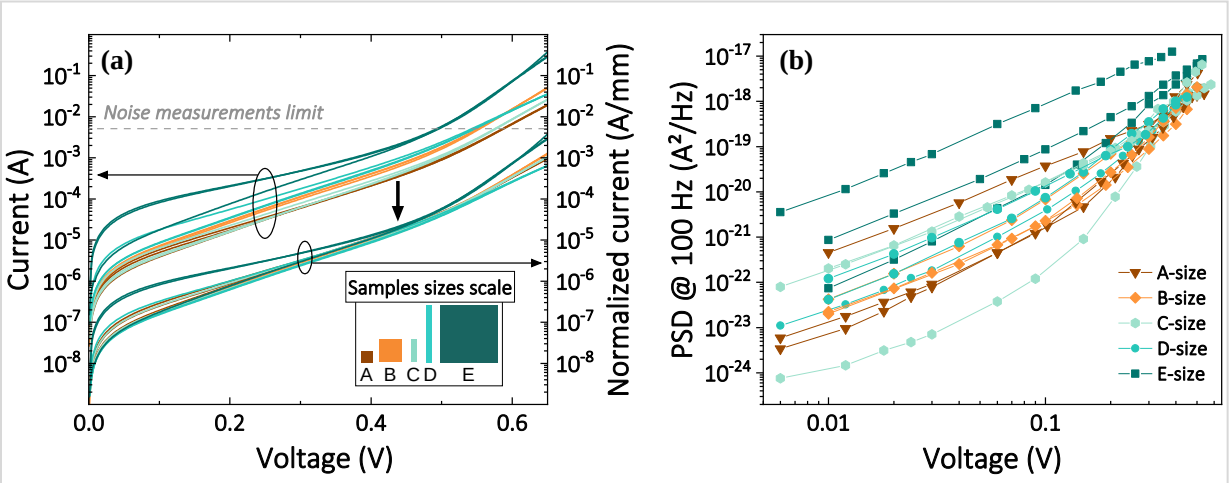

Figure 1: **(a)** Current-Voltage characteristics measured in fifteen samples (right), normalized by samples perimeter values (left). **(b)** Values of power spectral densities, showing a *Flicker noise*, extracted at 100 Hz as a function of the applied voltage in the same fifteen samples.

4.1 1/f noise induced by resistive shunt currents

Measurements presented in this section have been carried out on the E-shape sample (Table 1) which exhibited the highest noise level (Fig. 1-b), and it will be referred as *case #1*. Its current-voltage characteristic, presented in the inset of Fig. 2-a, is typical of a shunted solar cell, as a significant linear current is observed at low voltage, identical in forward and reverse bias. Current power spectral density measurements obtained on this sample between 6 mV and 420 mV are presented in Fig. 2-a. A *1/f* type noise can be observed in all spectra, with a flat region appearing at low frequencies. The slopes are fairly constant between spectra since the γ coefficient (Eq. (1.1)) is varying between 1.14 and 1.22. An average value of the PSD has been extracted around 100 Hz for each spectrum, and plotted against the voltage applied during the measurement (Fig. 2-b). It appears that the noise level is varying proportionally to the square of the voltage, as it would be the case for a Flicker noise source acting on a resistive current (Eq. (1.6)).

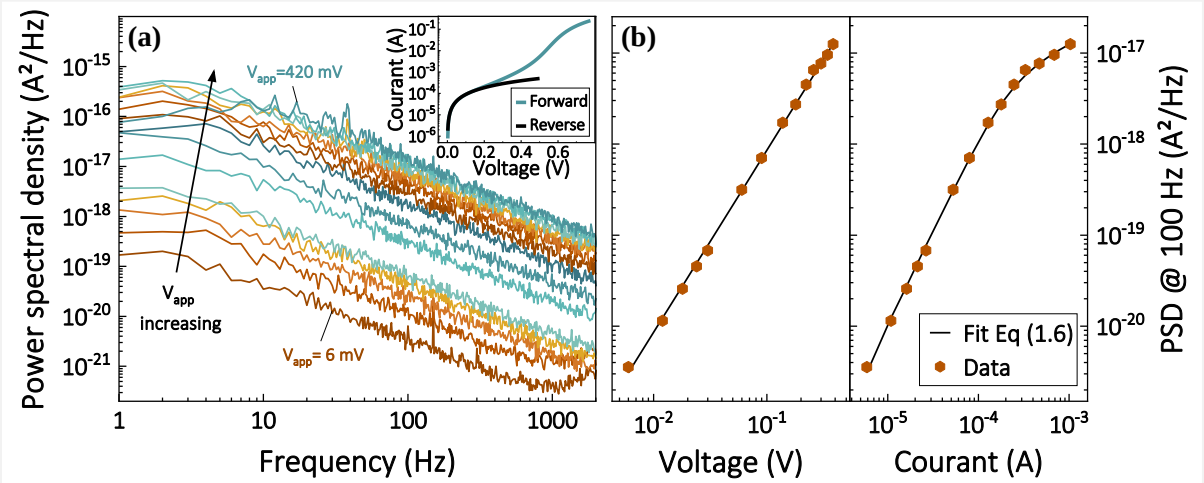

Figure 2: (a) Power spectral density curves at applied bias varying between 6 mV and 420 mV, *inset*: Current-Voltage characteristic in forward and reverse bias. (b) Power spectral density values extracted at 100 Hz as a function of the voltage (left) and the current (right). Experimental data was fitted according to Eq. (1.6) with a proportionality coefficient equal to 8.5×10^{-17} $S^2.Hz^{-1}$.

The current dependency of these PSD reinforces the hypothesis that the *1/f* noise measured is induced by the shunt currents in this sample. Indeed, the PSD is varying proportionally to the square of the current in the range in which the current is limited by the resistive conduction mechanism, and the curve is flattened when other conduction mechanisms begin to take precedence over it in the total current, without additional sources of fluctuation.

As it is represented in Fig. 3, showing the structure of the sample, it is likely that the measured *1/f* noise originates from conduction mechanisms enabled by fabrication-induced defects or structural damages locally reducing the effect of the space charge region. The nature of these defects can be of various types [37], and has not been specifically determined in the scope of this work.

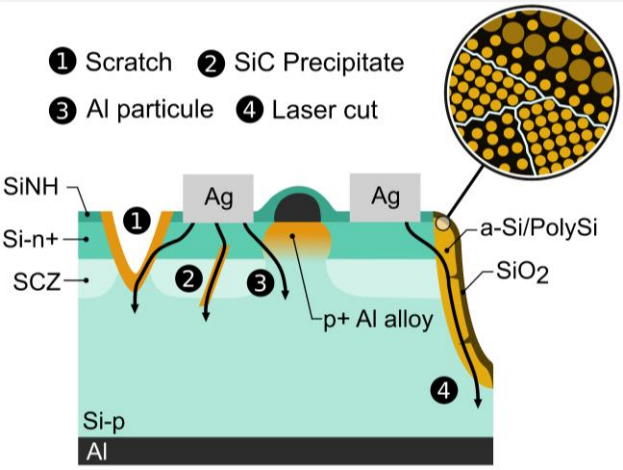

Figure 3: Representation of an Al-BSF solar cell structure (not at scale) with various structural defects inducing low voltage shunt currents. 1, 2 and 3 are three typical structural defects (scratch, SiC precipitate and Aluminum contamination) described in [37] that can induced local linear shunts current. 4 represents a laser cut inducing edges parasitic currents through a damaged layer of amorphized silicon, as observed in [44].

4.2 Identification and modeling of additional noise sources

For most of the samples, the *1/f* shunt noise model presented in the above section was not enough to explain alone the noise level on the range of bias studied. A second source of noise seems to appear at higher currents in samples with higher shunt resistances values. As highlighted in Fig. 1, this second tendency is emerging in a range of voltage bias for which the current is limited by a conduction mechanism occurring at the samples edges. Two physics-based modeling approaches to interpret this secondary noise contribution are presented in this section.

4.2.1 Tunnel current noise model

This sub-section is based on measurements carried out on a D-shape sample (Table 1) that will be referred as *case #2*. PSD measurements also revealed *1/f* type noise on a wide frequency range, whose values extracted at 100 Hz are presented in Fig. 4 as a function of the applied bias. It can be seen that the noise level measured for bias values higher than 100 mV does not match the *1/f* shunt noise model presented in section 3.1, whose voltage dependency follows solely V^2. This strongly suggests the presence of a secondary source of fluctuations as modelled by Eq. (1.9).

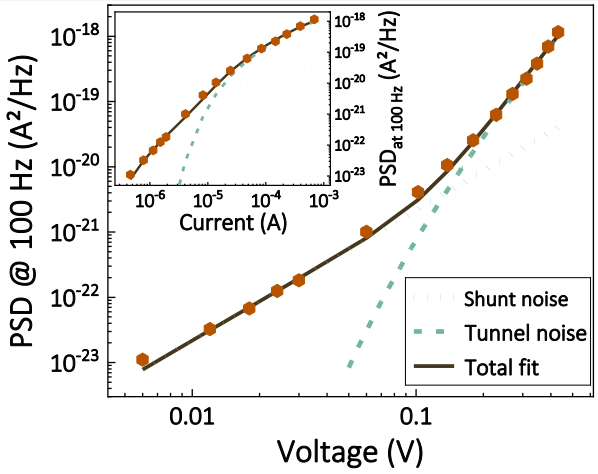

Figure 4: Power spectral density values extracted at 100 Hz as a function of the applied bias. The sum of the resistive *1/f* model and the tunnel current noise model presented in Eq. (3.3) is used to fit all data.

Based on the double diode model (Eq. (1.7)), the first assumption that could stem from these results is that the second diode would be a source of fluctuations. It appears however that the noise level is not increasing enough with voltage to correspond to a current varying exponentially, except if using an unrealistically high ideality factor, not matching the static IV characteristic of the cell. This second

noise trend rather seems to be approximatively proportional to V^4. According to the modelling developed in section 1.2, this would correspond to a current roughly proportional to V^2, as it would be the case for a tunnel current. Even if the samples structure is not supposed to contain oxide layers, it is possible that such layers have been formed during the laser cutting processes, as represented in Fig. 3. These defects could induce tunneling currents at the samples edges, that can be expressed in a simplified form according to the Fowler-Nordheim model [41] as:

$$I = C_1 V^2 \exp\left(-\frac{C_2}{V}\right) \tag{4.1}$$

where

$$\begin{cases} C_1 = \frac{q^3 m_{eff} A}{8\pi m_{diel} h q \Phi_1 t_{ox}^2} \\ C_2 = \frac{4 t_{ox} \sqrt{2 m_{diel} (q\Phi_1)^3}}{3\hbar q} \end{cases} \tag{4.2}$$

and A is the area crossed by the current, Φ_1 the potential barrier height, m_{eff} and m_{diel} the effective electron masses in the semiconductor and in the dielectric respectively and t_{ox} the thickness of the oxide layer.

In order to obtain a variation of the PSD proportional to V^4, it is necessary to assume that there is no quantity fluctuating in C_2. The only parameter that could fluctuate in C_1 is the effective surface through which the current flows, that would result from a modulation of the number of accessible conduction channels in the oxide layer. The equation describing the PSD could then be written as follow:

$$S_I = S_{C_1} V^4 \exp\left(-\frac{2C_2}{V}\right) \tag{4.3}$$

with S_{C_1} the fluctuation on C_1 expressed in $A^2.V^{-4}Hz^{-1}$. Such a model can provide a very good fit for high bias PSD values, as shown in Figure 4 for a value of C_2 equal to 0.088 V.

An additional element that seems to indicate the presence of a tunnel conduction mechanism has been provided by low-temperature IV measurements carried out on this sample, presented in Fig. 5. On the characteristic, a knee can be observed between 100 mV and 450 mV, typical of a tunnel current contribution. This knee can be very well approximated with a tunnel current term with the same parameter C_2 used to fit the PSD curves.

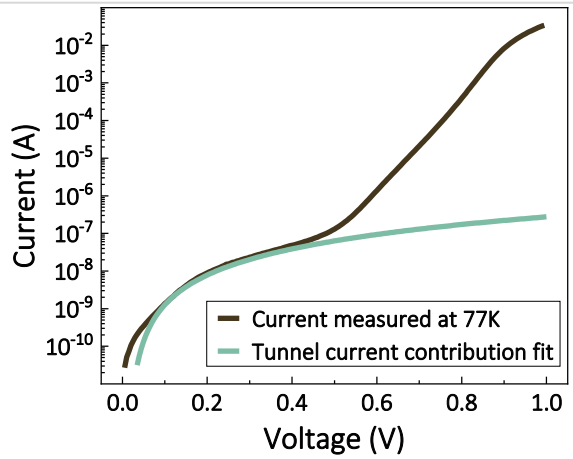

Figure 5. Current-Voltage characteristic measured at 77 K on sample n°2, and Fowler-Nordheim tunnel current model with C_2=0.088V.

Despite this very good agreement between the static and noise fit using the same parameters, there are elements nuancing the reliability of this first modeling approach. First of all, the fluctuation source in C_1 attributed to a modulation of the effective surface is questionable and hard to justify. Then, even if the cryogenic measurements give credibility to the existence of tunnel currents in these solar cells, the location of thin tunnel oxides in their structure is not clearly established.

Out of the six samples on which cryogenic measurements have been carried out, a knee in IV curves has only been observed on three samples. *Case #2* is the only one for which such a good match

has been obtained between values of C_2 extracted from noise and static measurements. The values of C_2 extracted from noise model are in addition below the range of the expected ones, even if the difference lies within less than one order of magnitude. Indeed, a minimal value for C_2 can be estimated to be around to 0.37 V, with t_{ox} =0.3 nm and Φ_1 = 0.4 eV, meanwhile the value found for case #2 was 0.088 V.

Finally, the fact that a conduction mechanism occurring several orders of magnitude under the measured current at 300 K would be responsible for the total measured noise measured is less likely, although not impossible as described by Eq. (1.9). An alternative interpretation and modeling approach is proposed in the next section, through the study of a third sample.

4.2.2 Poole-Frenkel noise model

This section will present the second approach used to interpret the noise results at the higher bias values, based on measurements obtained on the C-shape sample (Table 1) showing the lowest noise at low voltage (Fig. 1-b), referred to as case #3.

The Poole-Frenkel (PF) effect is a conduction mechanism resulting from the lowering of the potential barrier surrounding a trapping state under the effect of an applied electric field [42]. It is usually measured in disordered materials such as amorphous layers [43]. As described previously and represented in Fig. 3, it is likely that the cells edges were amorphized by the laser cuts as observed in [44], providing such conduction paths for charge carriers at low voltage. The Poole-Frenkel current density can be expressed as in [42]:

$$J_{PF} = \sigma_{PF}\,\vec{E}\exp\left(-\frac{q}{k_B T}\left(\Phi_B - \sqrt{\frac{qE}{\pi\epsilon}}\right)\right) \tag{4.4}$$

where $\sigma_{PF} = q\mu n$ is the PF conductivity, E the electric field, Φ_B the Coulombic potential barrier height. Assuming that the only fluctuating quantity is σ_{PF}, because of a fluctuation of either the mobility or the number of charge carriers, and that a thickness d could be defined such as $|E|=|V/d|$, the expected *1/f* power spectral density can be expressed as:

$$S_I = S_{PF} A_0^2 V^2 \exp\left(2B_0\sqrt{V}\right) \tag{4.5}$$

where:

$$\begin{cases} A_0 = \frac{S}{d}\exp\left(-\frac{q\Phi_B}{k_B T}\right) \\ B_0 = q\frac{\sqrt{q/\pi\epsilon d}}{k_B T} \end{cases} \tag{4.6}$$

and S_{PF} is the power spectral density of σ_{PF} expressed in $S^2.Hz^{-1}$.

The current power spectral densities measured for *case #3* between 6 mV and 500 mV are presented in Fig. 6-a. A first interesting observation is that a white noise contribution seems to appear on the first spectra, flattening the *1/f* noise measured at lower frequencies. It is very likely to correspond to a thermal noise in an equivalent resistor R, whose PSD is defined as:

$$S_I = 4k_B T/R \tag{4.7}$$

This phenomenon is observed in several measurements, and the resistance value extracted from the white noise level is matching the value of the shunt resistance extracted from static measurements in all of these cases. Even if the analysis of this white noise is limited due to a parasitic resonance phenomenon described in [40], it is likely that it stems from local resistive conductions in the low-doped base of the PV cell, enabled by structural defects such as those presented in Fig. 3. The current resulting from passing through these defects is then affected by both a *Flicker noise* induced by the latter (section 4.1), and a thermal noise due to the conduction in the base of the cell. These results greatly support the interest of the LFN analysis. Indeed, while the static measurement only gives information on the most resistive series conduction mechanism, the noise measurements can inform on the underlying ones. In *case* #1, the shunt resistance white noise impact is not visible in the measured spectra (Fig. 2-a), as its expected value is estimated to be around 1.55×10^{-23} A^2/Hz according to static

measurements, therefore negligible compared to the measured *1/f* noise.

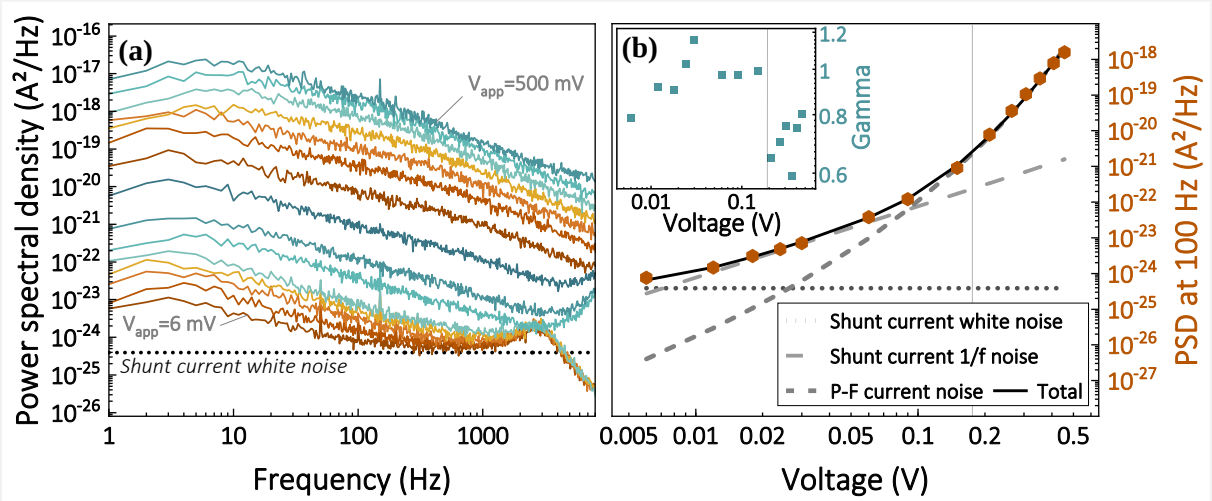

Figure. 6. **(a)** Power spectral density curves measured between 6 mV and 500 mV on sample n°3. The shunt current white noise was plotted for R_{sh}=42 kΩ. **(b)** Power spectral density values extracted from Fig.6-a at 100 Hz as a function of the applied bias.The estimations of the shunt current white noise, shunt current *1/f* noise and the Poole-Frenkel current noise adjusted with B_0=9.5V are plotted. Insert: *1/f* gamma coefficient as a function of the voltage

Fig. 6-b presents the PSD values at 100 Hz and the γ coefficients (Eq. (1.1)) of the *1/f* noise contribution observed between approximately 10 Hz and 150 Hz, as a function of the applied voltage. It appears that the thermal noise mentioned previously impacts the extraction of the three first PSD points, slightly above the estimation of the *1/f* shunt noise. The PSD values also deviate from this model for voltages above 100 mV, as in case #2. It is interesting to notice that this deviation corresponds very well to a change in γ from values around 1 to values around 0.7, supporting the hypothesis of two different distributions of defects or scattering centers. This additional noise at higher bias is very well fitted by Eq. (3.5), with a coefficient B_0 equal to 9.5 $V^{-1/2}$ for case #3, and between 5 and 10 $V^{-1/2}$ for all others. As represented in Fig. 3, it is possible that the charge carriers are able to shunt the SCZ thanks to the laser cut amorphized zones providing less resistive conduction paths.

As the static behavior of the solar cells studied in this paper could not be described by the two-diode model (ideality factor n_2 above 3 instead of n_2=2), the possible presence of a Poole-Frenkel current contribution suggested by the LFN behavior was examined for the Current-Voltages curves. It turned out that the characteristic of this sample at 300 K, presented in Figure 7, could be very well approximated with the following equation:

$$I(V) = \frac{V - IR_S}{R_{sh}} + A_0(V - IR_S)\exp\left(B_0\sqrt{V - IR_S}\right) + I_s\left(\exp\left(\frac{q(V-IR_S)}{nk_BT}\right) - 1\right) \qquad (4.8)$$

with B_0 equal to 10.07 $V^{-1/2}$, which is in very good agreement with the value of B_0 extracted from the noise fitting.

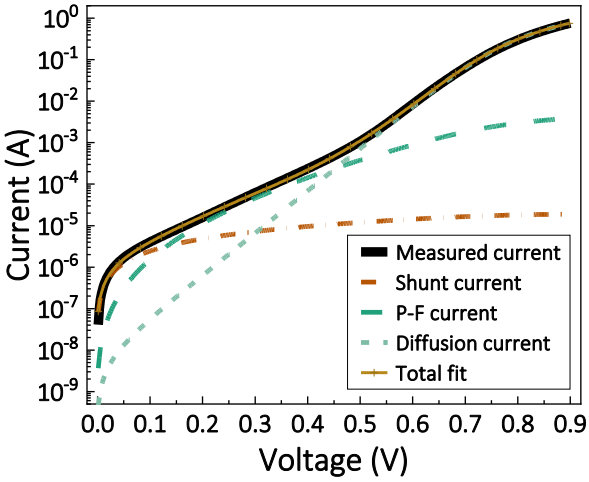

Figure 7: Current-Voltage characteristic measured on sample n°3 at 300 K, fitted according to (3.8), with each term of the equation plotted. The fitting parameters are: R_{sh}=42 kΩ, R_S=0.14 Ω, A_0=6×10^{-7} S, B_0=10.07 V$^{-1/2}$, I_S=5.5×10^{-9}A and n=1.68.

4.2.3 Cryogenic measurements

As the temperature dependence of the conduction mechanisms revealed by noise measurements is clearly identifiable, cryogenic measurements were performed on six samples. Current-Voltage characteristics between 77 K and 300 K measured on an A-shape sample (Table 1) and presented in Figure 8 are representative of the tendencies observed on most samples.

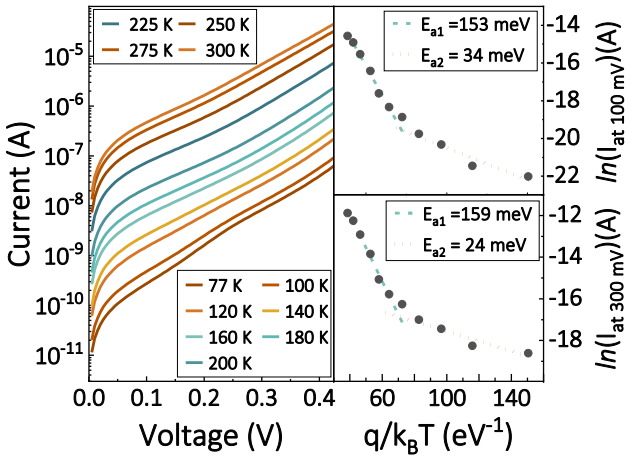

Figure 8: Current-Voltage characteristics measured on *sample n°4* between 77 K and 300 K (left) and logarithm of the current at 100 mV and 300 mV plotted against q/k_BT (right).

The current at 100 mV and 300 mV has been extracted for each curve in order to plot the logarithm of the current as a function of q/k_BT and to extract the activation energies of the conduction mechanisms involved. Two activation energies can be distinguished, around 155 meV for temperatures above 160 K and around 30 meV for lower temperatures. These activation energies, referred as E_{a1} and E_{a2}, are very low and typically observed in the presence of Poole-Frenkel and tunnel conductions respectively, as presented in [45] and [46]. These cryogenic measurements strongly support both hypotheses of fluctuation mechanisms presented above.

To summarize, the two conduction mechanisms identified thanks to the LFN experimental analysis and modeling are in very good agreement with the activation energies extracted from cryogenic measurements. One can therefore suggest that a combination of both mechanisms occurs at the damaged edges of the cells, responsible for the low-voltage current measured. Although the LFN analysis has strongly helped in the identification of these mechanisms, the analysis is limited by the fact that the intermixing of conduction mechanisms occurring in disordered materials is modeled using very simplified formulas, not necessarily reflecting their inherent complexity [5]. The Poole-Frenkel

conduction model has however provided a very good approximation of the static behavior of the cells at 300 K, and could thus constitute a convincing explanation of the abnormally high ideality factors generally observed at low bias in laser cut cells.

Conclusion

An analysis of the current and voltage variation of the 1/f noise level taking into account the multiplicity of parallel conduction mechanisms in PV components, coupled with static I-V-T measurements and suggested model approaches has been presented, leading to the identification of low voltage parasitic transport mechanisms in laser cut Al-BSF cells. A first LFN contribution has been linked to local linear shunt phenomena, regularly observed in PV cells. A second noise contribution was identified for higher currents, arising from conduction through the diced sample edges, via either tunneling or Poole-Frenkel effect. Cryogenic measurement results suggested that the conduction at the edge of the samples could be a complex combination of both mechanisms. The Poole-Frenkel approach also provides a very good approximation of the nonlinear parasitic current measured at low voltage, which can explain the abnormally high ideality factor extracted if a g-r current is assumed instead. The observed results have confirmed the precaution needed when dicing PV samples due to the induced low voltage parasitic conduction mechanisms, and highlight the importance of the presented method as a significant additional tool for the characterization of electronic transport and defective zones in PV cells.

Acknowledgements

This work was supported by the French National Research Agency (OXYGENE 17-CE05-0034 and BRIGHTSIDE 22-CE05-0027 projects).

References

[1] Fraunhofer Institute for Solar Energy Systems ISE, “Photovoltaics Report,” 2022. Accessed: Sep. 07, 2022. [Online]. Available: www.ise.fraunhofer.de.

[2] R. H. Hopkins and A. Rohatgi, “IMPURITY EFFECTS IN SILICON FOR HIGH EFFICIENCY SOLAR CELLS,” *J. Cryst. Growth*, vol. 75, pp. 67–79, 1986.

[3] C. T. Sah, R. N. Noyce, and W. Shockley, “Carrier Generation and Recombination in P-N Junctions and P-N Junction Characteristics,” *Proc. IRE*, vol. 45, no. 9, pp. 1228–1243, 1957, doi: 10.1109/JRPROC.1957.278528.

[4] K. Rühle, M. K. Juhl, M. D. Abbott, and M. Kasemann, “Evaluating Crystalline Silicon Solar Cells at Low Light Intensities Using Intensity-Dependent Analysis of I-V Parameters,” *IEEE J. Photovoltaics*, vol. 5, no. 3, pp. 926–931, May 2015, doi: 10.1109/JPHOTOV.2015.2395145.

[5] O. Breitenstein, P. Altermatt, K. Ramspeck, M. A. Green, J. Zhao, and A. Schenk, “Interpretation of the commonly observed I-V characteristics of C-SI cells having ideality factor larger than two,” in *Conference Record of the 2006 IEEE 4th World Conference on Photovoltaic Energy Conversion, WCPEC-4*, 2006, vol. 1, pp. 879–884, doi: 10.1109/WCPEC.2006.279597.

[6] A. Kaminski, J. J. Marchand, and A. Laugier, “Non ideal dark I-V curves behavior of silicon solar cells,” 1998.

[7] K. R. Mcintosh and C. B. Honsberg, “The Influence of Edge Recombination on a Solar Cell’s Iv Curve THE INFLUENCE OF EDGE RECOMBINATION ON A SOLAR CELL’S I{V CURVE,” 2000, Accessed: Jan. 17, 2023. [Online]. Available: https://www.researchgate.net/publication/247910506.

[8] R. Jayaraman and C. G. Sodini, “1/F Noise Technique To Extract the Oxide Trap Density Near the Conduction Band Edge of Silicon,” *IEEE Trans. Electron Devices*, vol. 36, no. 9 pt 1, pp. 1773–1782, 1989, doi: 10.1109/16.34242.

[9] T. G. M. Kleinpenning, “ 1/ F Noise in P - N Junction Diodes ,” *J. Vac. Sci. Technol. A Vacuum, Surfaces, Film.*, vol. 3, no. 1, pp. 176–182, 1985, doi: 10.1116/1.573194.

[10] B. Sopori, “Silicon solar-cell processing for minimizing the influence of impurities and defects,” *J. Electron. Mater.*, vol. 31, no. 10 SPEC., pp. 972–980, 2002, doi: 10.1007/S11664-002-0030-X/METRICS.

[11] A. Van Der Ziel, “Flicker Noise in Electronic Devices,” *Adv. Electron. Electron Phys.*, vol. 49, no. C, pp. 225–297, Jan. 1979, doi: 10.1016/S0065-2539(08)60768-4.

[12] F. N. Hooge, “1/f noise is no surface effect,” *Phys. Lett. A*, vol. 29, no. 3, pp. 139–140, Apr. 1969, doi: 10.1016/0375-9601(69)90076-0.

[13] K. M. Van Vliet, “Noise and Admittance of the Generation—Recombination Current Involving Srh Centers in the Space-Charge Region of Junction Devices,” *IEEE Trans. Electron Devices*, vol. 23, no. 11, pp. 1236–1246, 1976, doi: 10.1109/T-ED.1976.18585.

[14] P. O. Lauritzen, “Noise Due to Generation and Recombination of Carriers in p-n Junction Transition Regions,” *IEEE Trans. Electron Devices*, vol. 15, no. 10, pp. 770–776, 1968, doi: 10.1109/T-ED.1968.16513.

[15] A. L. McWhorter and R. H. Kingston, *Semiconductor Surface Physics*. 1957.

[16] D. V Kuksenkov, H. Temkin, and A. Osinsky, “Low-frequency noise and performance of GaN junction photodetectors ARTICLES YOU MAY BE INTERESTED IN,” *J. Appl. Phys.*, vol. 83, p. 2142, 1998, doi:

10.1063/1.366950.
[17] S. T. Hsu, “Surface state related 1 f noise in p-n junctions,” *Solid State Electron.*, vol. 13, no. 6, pp. 843–855, Jun. 1970, doi: 10.1016/0038-1101(70)90070-5.
[18] G. Landi, C. Barone, C. Mauro, H. C. Neitzert, and S. Pagano, “A noise model for the evaluation of defect states in solar cells,” *Sci. Rep.*, vol. 6, pp. 1–9, Jul. 2016, doi: 10.1038/srep29685.
[19] Z. Chobola, “Noise as a tool for non-destructive testing of single-crystal silicon solar cells,” *Microelectron. Reliab.*, vol. 41, no. 12, pp. 1947–1952, 2001, doi: 10.1016/S0026-2714(01)00219-0.
[20] L. K. J. Vandamme, R. Alabedra, and M. Zommiti, “1/F Noise As a Reliability Estimation for Solar Cells,” *Solid State Electron.*, vol. 26, no. 7, pp. 671–674, 1983, doi: 10.1016/0038-1101(83)90023-0.
[21] N. Papež *et al.*, “Degradation analysis of GaAs solar cells at thermal stress,” 2018, doi: 10.1016/j.apsusc.2018.05.093.
[22] K. Davenport, C. T. Trinh, M. Hayward, K. Lips, and A. Rogachev, “Relaxation processes in silicon heterojunction solar cells probed via noise spectroscopy,” *Sci. Reports* |, vol. 11, p. 13238, 123AD, doi: 10.1038/s41598-021-92866-w.
[23] D. Cho, T. Hwang, D.-G. Cho, B. Park, and S. Hong, “Photoconductive noise microscopy revealing quantitative effect of localized electronic traps on the perovskite-based solar cell performance,” 2017, doi: 10.1016/j.nanoen.2017.11.009.
[24] V. K. Sangwan *et al.*, “Low-Frequency Carrier Kinetics in Perovskite Solar Cells,” *ACS Appl. Mater. Interfaces*, vol. 11, no. 15, pp. 14166–14174, Apr. 2019, doi: 10.1021/acsami.9b03884.
[25] H.-C. Neitzert, “Noise characterization of perovskite solar cells,” *https://doi-org.gaelnomade-1.grenet.fr/10.1117/12.2306100*, vol. 10533, pp. 100–106, Feb. 2018, doi: 10.1117/12.2306100.
[26] A. Singh *et al.*, “Insights Into the Microscopic and Degradation Processes in Hybrid Perovskite Solar Cells Using Noise Spectroscopy,” *Sol. RRL*, vol. 2, no. 1, p. 1700173, Jan. 2018, doi: 10.1002/SOLR.201700173.
[27] C. Barone *et al.*, “Unravelling the low-temperature metastable state in perovskite solar cells by noise spectroscopy,” *Sci. Rep.*, vol. 6, no. July, pp. 1–8, Oct. 2016, doi: 10.1038/srep34675.
[28] Q. Shen *et al.*, “Characterization of Low-Frequency Excess Noise in CH3NH3PbI3-Based Solar Cells Grown by Solution and Hybrid Chemical Vapor Deposition Techniques,” *ACS Appl. Mater. Interfaces*, vol. 10, no. 1, pp. 371–380, Jan. 2018, doi: 10.1021/acsami.7b10091.
[29] A. K. Mishra and R. K. Shukla ⇑, “Effect of humidity in the perovskite solar cell,” doi: 10.1016/j.matpr.2020.04.872.
[30] K. Kaku, A. T. Williams, B. G. Mendis, and C. Groves, “Examining charge transport networks in organic bulk heterojunction photovoltaic diodes using 1/f noise spectroscopy †,” *J. Mater. Chem. C*, vol. 3, p. 6077, 2015, doi: 10.1039/c5tc00348b.
[31] H. Katsu, Y. Kawasugi, R. Yamada, and H. Tada, “Low frequency noise in organic solar cells,” *Proc. IEEE 21st Int. Conf. Noise Fluctuations, ICNF 2011*, pp. 77–79, 2011, doi: 10.1109/ICNF.2011.5994389.
[32] C. Barone, G. Landi, A. De Sio, H. C. Neitzert, and S. Pagano, “Thermal ageing of bulk heterojunction polymer solar cells investigated by electric noise analysis,” *Sol. Energy Mater. Sol. Cells*, vol. 122, pp. 40–45, Mar. 2014, doi: 10.1016/j.solmat.2013.11.020.
[33] K. A. Luck *et al.*, “Correlated In Situ Low-Frequency Noise and Impedance Spectroscopy Reveal Recombination Dynamics in Organic Solar Cells Using Fullerene and Non-Fullerene Acceptors,” *Adv. Funct. Mater.*, vol. 27, no. 48, p. 1703805, Dec. 2017, doi: 10.1002/ADFM.201703805.
[34] L. Li, Y. Shen, and J. C. Campbell, “The impact of thermal annealing temperature on the low-frequency noise characteristics of P3HT:PCBM bulk heterojunction organic solar cells,” *Sol. Energy Mater. Sol. Cells*, vol. 130, pp. 151–155, Nov. 2014, doi: 10.1016/J.SOLMAT.2014.07.009.
[35] M. Joodaki and M. Salari, “Investigation of the tensile strain influence on flicker noise of organic solar cells under dark condition,” *Org. Electron.*, vol. 59, pp. 230–235, Aug. 2018, doi: 10.1016/J.ORGEL.2018.05.018.
[36] Y. Liu, S. Wang, L.-M. Peng, Y. Liu, L.-M. Peng, and S. Wang, “Toward High-Performance Carbon Nanotube Photovoltaic Devices,” *Adv. Energy Mater.*, vol. 6, no. 17, p. 1600522, Sep. 2016, doi: 10.1002/AENM.201600522.
[37] O. Breitenstein, J. P. Rakotoniaina, M. H. Al Rifai, and M. Werner, “Shunt types in crystalline silicon solar cells,” *Prog. Photovoltaics Res. Appl.*, vol. 12, no. 7, pp. 529–538, Nov. 2004, doi: 10.1002/PIP.544.
[38] T. Desrues *et al.*, “High quality industrial phosphorus emitter doping obtained with innovative plasma immersion ion implantation (PIII) processes,” *Proceeding 33rd Eur. Photovolt. Sol. Energy Conf. Exhib. Amsterdam*, 2017.
[39] J. A. Chroboczek and G. Piantino, “Programmable gain and bias low-noise current amplifier,” France Patent No. 15075, 1999.
[40] C. Wulles, Q. Rafhay, T. Desrues, A. Kaminski, and C. Theodorou, “Parasitic oscillation in the low-frequency noise characterization of solar cells,” *Solid. State. Electron.*, vol. 194, p. 108327, Aug. 2022, doi: 10.1016/j.sse.2022.108327.
[41] Z. A. Weinberg, “On tunneling in metal-oxide-silicon structures,” *J. Appl. Phys.*, vol. 53, p. 5052, 1982, doi: 10.1063/1.331336.
[42] J. R. Yeargan and H. L. Taylor, “The Poole-Frenkel effect with compensation present,” *J. Appl. Phys.*, vol. 39, no. 12, pp. 5600–5604, 1968, doi: 10.1063/1.1656022.
[43] A. K. Jonscher, “Reviews ELECTRONIC PROPERTIES OF AMORPHOUS DIELECTRIC FILMS.”
[44] J. Kaspar, A. Luft, S. Nolte, M. Will, and E. Beyer, “Laser helical drilling of silicon wafers with ns to fs pulses: Scanning electron microscopy and transmission electron microscopy characterization of drilled through-holes,” *J. Laser Appl.*, vol. 18, no. 2, pp. 85–92, May 2006, doi: 10.2351/1.2164480.
[45] N. M. Johnson and C. G. V. de Walle, “Chapter 2: Isolated Monatomic Hydrogen in Silicon,” in *Semiconductors and Semimetals*, vol. 61, no. C, Academic Press Inc., 1999, pp. 13–23.

[46] C. H. Lin, B. C. Hsu, M. H. Lee, and C. W. Liu, “A comprehensive study of inversion current in MOS tunneling diodes,” *IEEE Trans. Electron Devices*, vol. 48, no. 9, pp. 2125–2130, Sep. 2001, doi: 10.1109/16.944205.